

Spatial flow structure around a smooth circular cylinder in the critical Reynolds number regime under cross-flow condition

Arash Raeesi*, Shaohong Cheng[‡] and David S-K. Ting^{†‡}

University of Windsor, 401 Sunset Ave., Windsor, ON., Canada N9B 3P4

(Received March 28, 2008, Accepted May 17, 2008)

Abstract. The spanwise flow structure around a rigid smooth circular cylinder model in cross-flow has been investigated based on the experimental data obtained from a series of wind tunnel tests. Surface pressures were collected at five spanwise locations along the cylinder over a Reynolds number range of 1.14×10^5 to 5.85×10^5 , which covered sub-critical, single-bubble and two-bubble regimes in the critical range. Separation angles were deduced from curve fitted to the surface pressure data. In addition, spanwise correlations and power spectra analyses were employed to study the spatial structure of flow. Results at different spanwise locations show that the transition into single-bubble and two-bubble regimes could occur at marginally different Reynolds numbers which expresses the presence of overlap regions in between the single-bubble regime and its former and later regimes. This indicates the existence of three-dimensional flow around the circular cylinder in cross-flow, which is also supported by the observed cell-like surface pressure patterns. Relatively strong spanwise correlation of the flow characteristics is observed before each transition within the critical regime, or formation of first and second separation-bubbles. It is also noted that these organized flow structures might lead to greater overall aerodynamic forces on a circular cylinder in cross-flow within the critical Reynolds number regime.

Keywords: circular cylinder; critical Reynolds number regime; cross-flow, spanwise variation; separation angle.

1. Introduction

Flow past a circular cylinder is one of the fundamental topics in fluid dynamics. It deserves great attention because it is a common scenario in everyday life and in many engineering applications, such as wind past the strings of a wind harp or cables on cable-stayed bridges, ocean current past marine guy cables, or flow past pipes in heat exchangers. A decent knowledge of flow pattern around such a simple bluff body in the smooth flow condition is a priori to explore the effects of complex turbulent flow, such as natural wind, on the practical cylindrical type of structures (Simiu and Scanlan 1996). Though intensive effort has been invested in advancing this evergreen topic for

* Dept. of Mechanical, Automotive & Materials Engineering, Graduate student, E-mail: raeesi@uwindsor.ca

‡ Dept. of Civil & Environmental Engineering, Assistant Professor, Corresponding author, E-mail: shaohong@uwindsor.ca

†‡ Dept. of Mechanical, Automotive & Materials Engineering, Professor, E-mail: dting@uwindsor.ca

over a century, some aspects of the phenomenon are still far from comprehension. In particular, studies on the spatial variation of flow structure around a circular cylinder, be it normal or inclined to the oncoming flow direction, are rarely seen in the literature, yet the knowledge would be central to the understanding of the basic physics underlying various types of flow-induced responses of a circular cylinder.

Majority of the previous studies on flow past a circular cylinder were conducted based on the aerodynamic data at one particular location along the cylinder span, without revelation of spatial variation. Roshko (1961) first attempted to classify the characteristics of cross-flow past a circular cylinder at very high Reynolds numbers regime, where he defined different flow states for Reynolds numbers in excess of 1×10^5 as sub-critical ($C_d \approx 1.2$), supercritical (C_d value drastically reduces to about 0.3), and transcritical ($C_d \approx 0.7$). Within each sub-range, the flow exhibits different features of aerodynamic characteristics. He also found that the regular periodic vortex shedding, which ceased in the supercritical regime, reappeared in the transcritical regime. Roshko's findings and the existence of different sub-regimes which he defined were reconfirmed later by a number of researchers including Achenbach (1968), Bearman (1969), Batham (1972) and Schewe (1983). Zdravkovich (1997) made a comprehensive review for a broad range of researches done on this subject, where he used the notation "TrBL" (transition in boundary layer) to represent the Reynolds numbers ranging from 1×10^5 up to a few millions (within which the current experimental study was conducted). This range was subdivided into TrBL0 as the sub- or pre-critical regime ($1 \sim 2 \times 10^5 < Re < 3 \sim 3.4 \times 10^5$); TrBL1 as the single separation-bubble regime with steady asymmetric pressure distribution ($3 \sim 3.4 \times 10^5 < Re < 3.8 \sim 4 \times 10^5$); TrBL2 as the range accompanied with the formation of the second separation-bubble and return of the flow symmetry ($3.8 \sim 4 \times 10^5 < Re < 5 \sim 10 \times 10^5$); TrBL3 as the supercritical regime where the regular vortex shedding ceases ($5 \sim 10 \times 10^5 < Re < 3.6 \sim 6 \times 10^6$) and TrBL4 as the post- or transcritical regime which is followed by reappearance of the periodic vortex shedding ($Re > 3.6 \sim 6 \times 10^6$). To be consistent with other literatures, Zdravkovich's classification is used in the present paper and the term "critical Reynolds number regime" will be used to represent TrBL1 and TrBL2 regimes.

Bearman (1969) observed a steady lift force as a consequence of asymmetric flow structure around a circular cylinder within a narrow range of critical Reynolds number. He suggested that this steady lift force could be induced by the formation of laminar separation bubble on just one side of the cylinder surface within that particular Reynolds number range. Beyond that range, the second separation bubble would appear on the other side, the flow structure would become symmetric again and the steady lift force would then return to zero. Schewe (1983) confirmed Bearman's findings and proposed an associated mechanism. According to him, the transition in the boundary layer depended on the micro-scale perturbations which would not occur necessarily on both sides of the cylinder surface simultaneously. Therefore, the formation of the first separation bubble on one side of the cylinder surface would cause a steady circulation around the cylinder and decelerate the flow over the opposite side. The transition and formation of the second separation bubble on the other side would thus be delayed. It should also be noted that different aspects of fluctuating lift force on a circular cylinders have been studied in a very comprehensive and recent review by Norberg (2003), within which his own measurements in the subcritical range (Re up to 2.1×10^5) were compiled.

The three-dimensional structure of the flow around a circular cylinder, whether normal or inclined to the oncoming flow, was only addressed in a limited number of studies. For the case of a cross-flow cylinder, Roshko (1954) first observed three-dimensional structures of flow (in terms of either slanted or wavy spanwise eddy filaments) at Reynolds numbers as low as around 100. It was later found that (Slaouti and Gerrard, 1980) subtle difference in boundary conditions at the two ends can

cause the flow characteristics to vary along the cylinder span. Spanwise correlation length, i.e. the maximum length along which correlation coefficient of sectional aerodynamic characteristics is not lost, is another feature of three-dimensional flow. Within the subcritical Reynolds numbers range, the spanwise correlation length could be found in the study by Norberg (2001) and references cited in it. It was shown that within the subcritical Re range, the spanwise correlation length has a general decreasing trend with increase of Reynolds number except for a local maximum at $Re = 5 \times 10^3$ (Norberg 2001). Other studies addressing such three-dimensional structures in either wake or shear layers were reviewed by Roshko (1993) and later by Williamson (1997). Most of them were conducted in the subcritical Re range by flow visualization.

At higher Reynolds numbers, when the transition in boundary layer occurs, the impact of perturbations on the three-dimensional structure of the flow around a cross-flow circular cylinder was identified by Bearman (1969). Further, it was noticed that as the surrounding flow become three-dimensional, the cylinder base pressure is no longer uniform along the cylinder span. Based on the force measurement at both ends of the circular cylinder in the critical Reynolds number regime, Schewe (1983) suggested that the flow field around a circular cylinder in cross-flow could be divided along its span into many subsystems, which would differ slightly from each other in terms of aerodynamic characteristics. To the knowledge of the authors, there have been very few studies dedicated to investigate such three-dimensionalities at Reynolds numbers corresponding to the critical regime. Higuchi, *et al.* (1989) conducted experiments over a range of Re from 0.8×10^5 to 2×10^5 . They found that flow motion in this regime is characterized by the intermittent boundary-layer separation and reattachment accompanied with the presence of well-defined spanwise cell structures. Different spanwise structures were also observed in the flow visualizations by Humphreys (1960), Korotkin (1976), and more recently, Gölling (2004) within the TrBL regime. It is clear from these studies that much is yet to be uncovered regarding the three-dimensional structure of flow around a circular cylinder, especially in the critical Reynolds number regime.

The present work focuses on studying the spatial structure of flow pattern around a circular cylinder in cross-flow. The analysis is based on the experimental data of a wind tunnel test conducted earlier by Cheng and Tanaka (2005). Surface pressure was measured at five different longitudinal locations along the cylinder span, at fourteen Reynolds numbers in the TrBL regime from 1.14×10^5 to 5.85×10^5 . Fluctuating flow characteristics such as the separation angle and aerodynamic forces at those five locations and their spanwise correlations are analyzed. The possible existence of multiple flow regimes at different spanwise locations as suggested by Schewe (1983) is also discussed.

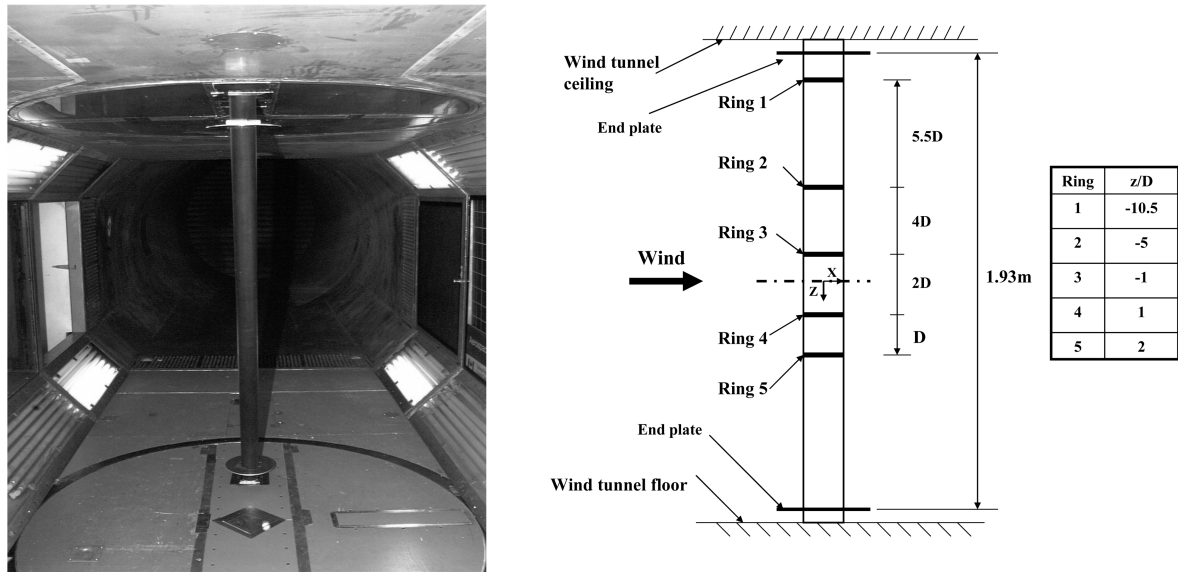
2. Experimental details

A series of wind tunnel tests has been conducted at National Research Council of Canada (NRCC) for studying wind-induced vibration of bridge stay cables by using a rigid smooth circular cylinder model (Cheng and Tanaka 2005). The current study is based on the experimental data obtained from this set of experiments.

The tests were conducted under smooth flow condition in the 2 m high by 3 m wide wind tunnel at NRCC. The maximum wind speed of the tunnel is 140 m/s. To simulate the cross flow case, a rigid steel circular cylinder model with a diameter of 88.9mm was installed vertically across the center of the test section and placed perpendicular to the on-coming flow direction, as shown in Fig. 1(a). Elliptical plates were attached close to both ends of the model to reduce the horse-shoe vortex and boundary-layer end effects. The exposed length of the cylinder to the flow in between the end

plates was 1.93 m. This leads to a model aspect ratio of 21.7. The blockage ratio is 2.96%.

To monitor the flow pattern around the cylinder model, a total of 192 pressure taps of 1mm diameter were installed on the model. As illustrated in Fig. 1(b), five pressure tap rings were fitted at different longitudinal locations along the cylinder span (Z direction), with the plane of each ring perpendicular to the model axis. Each ring contains 32 pressure taps over the circumference of the model with a more condensed arrangement on the downstream side. Fig. 2 portrays the layout of pressure taps on a typical ring and the definition of the X and Y axes with respect to the on-coming



(a) Cross-flow circular cylinder model in the NRCC wind tunnel

(b) Arrangement of pressure tap rings along the cylinder span

Fig. 1 Experimental setup

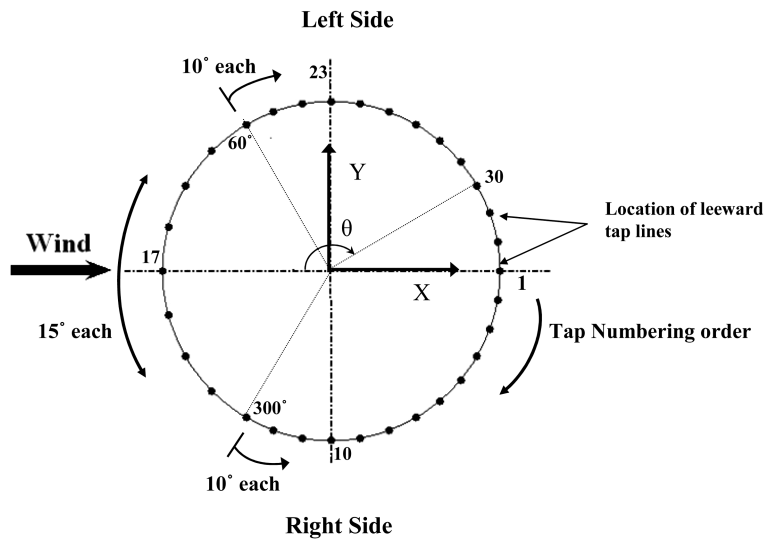


Fig. 2 Tap array around cylinder circumference on a typical ring

wind direction. The angular positions are defined clockwise, with respect to the location of tap number 17. Also, left and right sides of the cylinder are defined in Fig. 2 with respect to the wind direction. In addition, 32 pressure taps were installed along two longitudinal lines at the leeward side of the model, with 16 taps on each line. The pressure taps were connected to five electronic pressure scanners (Scanivalve ZOC™Kulite) embedded in the model through urethane tubes, nominally 1m long.

The tests were conducted under smooth flow conditions, with the longitudinal turbulence intensity at the model location being 0.13%. Unsteady surface pressure of the cylinder model at the tap locations were measured over a wind tunnel speed range of 19.6 m/s to 98.6 m/s, which, based on the cylinder diameter, corresponded to a Reynolds number range of 1.14×10^5 to 5.85×10^5 . Two sampling frequencies of 400Hz and 1200Hz were used, with details described in Table 1. The distortion of the sampled pressure signals induced by the tubing system was corrected before further analyses of the collected data. Due to the relatively low percentage of blockage ratio, no correction of blockage effect was made to the raw data. More details regarding this series of wind tunnel experiments are reported by Cheng and Tanaka (2005).

Table 1 Experimental conditions

Sampling mode	Sampling frequency (Hz)	Testing cases	Re range	Sampling time(S)	Activated taps	No. of active taps
Low	400	14	1.14×10^5 to 5.85×10^5	120	At 5 rings + 2 lines	192
High	1200	12	1.14×10^5 to 5.85×10^5	60	Rings 2 and 4	64

3. Results and discussion

In order to study the spatial structure of flow past a circular cylinder in the critical Reynolds number range, the surface pressure time-histories are further processed to obtain parameters that are key to the representation of the surrounding flow structure. The time-averaged surface pressure of the cylinder, time-averaged separation angles, power spectra of fluctuating separation angles, and the spanwise correlations of separation angles, force coefficients and surface pressures are presented in the following sections.

3.1. Surface pressure distributions

3.1.1. Time-averaged surface pressure

The time-averaged cylinder surface pressures at the locations of all five rings are presented in Fig. 3. The dimensionless pressure coefficient is represented by $C_p = P / (0.5\rho V^2)$, where V is the wind tunnel speed, ρ is the air density, and P is the measured gauge pressure. Fig. 3(a) portrays the time-averaged surface pressure at $Re = 1.14 \times 10^5$, which is within the TrBL0 (sub-critical) regime. It can be seen from the figure that the surface pressure around the cylinder circumference shows almost the same distribution at all five spanwise locations considered. This indicates that the flow structure in this Reynolds number range is primarily two-dimensional which agrees with many earlier studies (Fage 1928, Achenbach 1968, Batham 1972). Distribution of the time-averaged surface pressure at $Re = 3.04 \times 10^5$ is illustrated in Fig. 3(b), which corresponds to the TrBL1 regime. A highly asymmetric steady pressure distribution can be observed particularly at the spanwise locations of

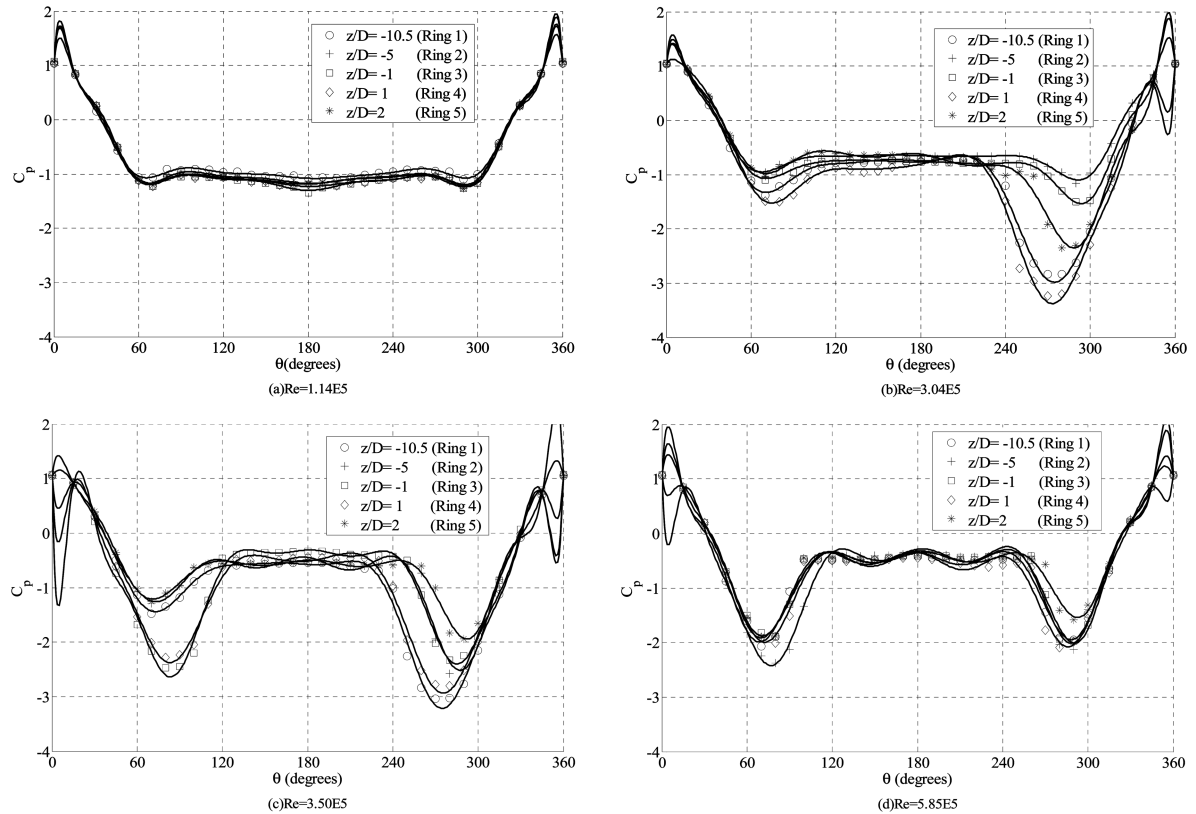


Fig. 3 Time-averaged surface pressures of five spanwise locations at four Reynolds numbers (Note: For the purpose of deriving separation angles, curve fitting was applied to the sampled surface pressure data by 16th order polynomial. The solid lines in the figure show the fitted curves, with details presented in Section 3.2.1)

Rings 1, 4 and 5 (where $z/D = -10.5, 1, 2$ respectively). This fact correlates to the formation of a single separation bubble on one side of the cylinder surface, which is the phenomenon to be expected in the TrBL1 regime, as was observed by Bearman (1969) and Schewe (1983). When the Reynolds number increases to 3.50×10^5 , the symmetric circumferential pressure distribution reappears at some spanwise locations (at $z/D = -1$ and 1), as shown in Fig. 3(c). This indicates the formation of the second separation bubble on the other side of the cylinder surface at those locations. Fig. 3(d) shows the time-averaged surface pressure distribution at $Re = 5.85 \times 10^5$. It is accompanied by a decrease of the minimum pressure coefficient at all spanwise locations considered (e.g. at Ring 4, from $|C_{p, \min}| \approx 3.0$ in Fig. 3(c) to $|C_{p, \min}| \approx 2.0$ in Fig. 3(d)).

Differences between time-averaged circumferential pressure distributions at different spanwise locations when the flow undergoes transition from TrBL0 to TrBL1 or from TrBL1 to TrBL2 regime can be seen in Fig. 3. In Fig. 3(b), surface pressure distribution at $z/D = -10.5, 1$ and 2 (locations of Rings 1, 4 and 5) show significant asymmetry, while at $z/D = -5$ and -1 (locations of Rings 2 and 3), they still remain more or less symmetric. At $Re = 3.50 \times 10^5$, as shown in Fig. 3(c), the reappearance of symmetric pressure distribution can only be detected at $z/D = -1$ and 1 (locations of Rings 3 and 4). While at higher Reynolds numbers, the symmetric pressure distribution around the circumference of the

cylinder more or less reoccur at all spanwise locations considered. The existence of both symmetric and asymmetric circumferential pressure distributions in Fig. 3(b) and Fig. 3(c) suggests the co-existence of dual flow sub-regimes along the span of a circular cylinder in a narrow critical Reynolds number range.

3.1.2. Surface pressure contours

Surface pressure contours detected from the time-averaged pressure data are plotted in Fig. 4. The vertical axis represents dimensionless distance from the midspan of the cylinder to the location of different rings, z/D . The horizontal axis gives the angular position in terms of the circumferential angle, θ .

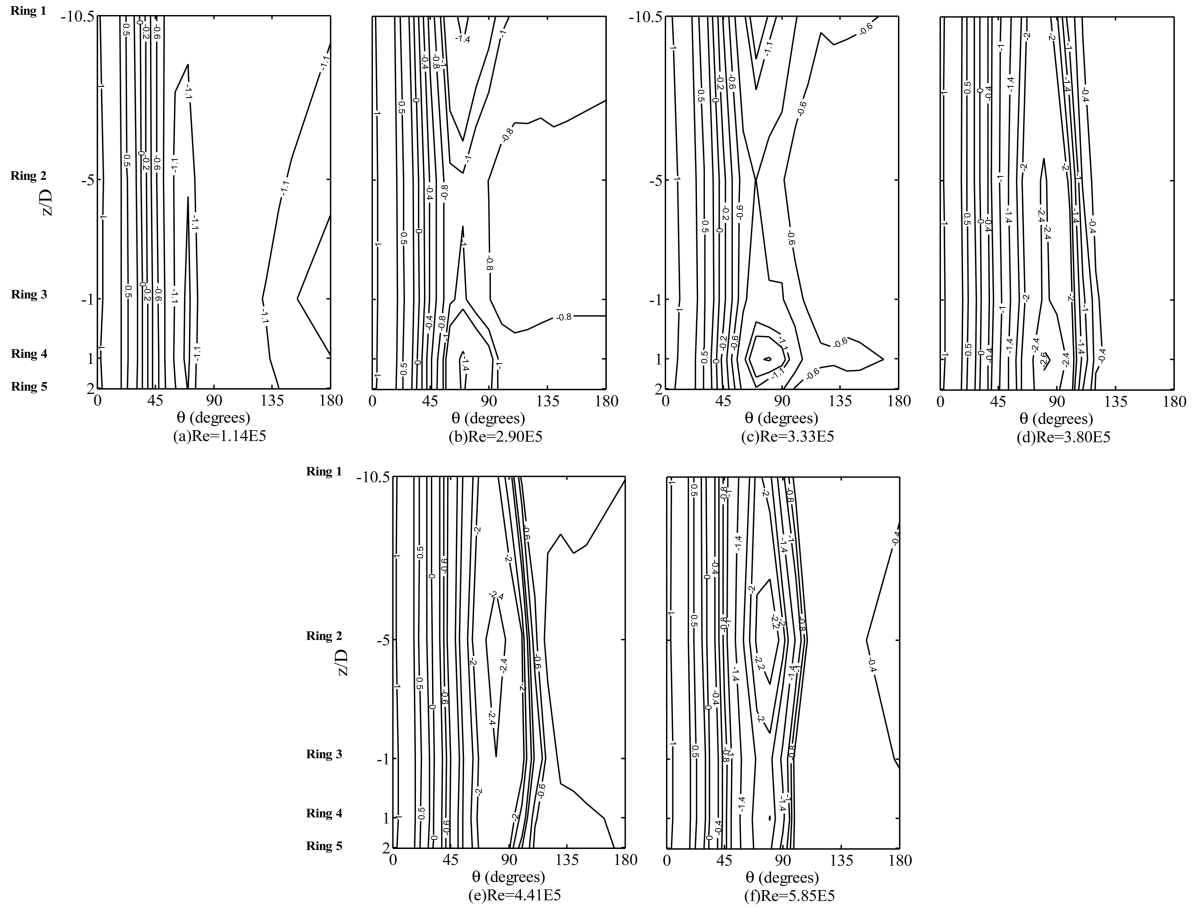
Fig. 4(a) illustrates pressure contours within the sub-critical regime at $Re = 1.14 \times 10^5$. As expected, constant spanwise pressure patterns, as indicated by fairly straight (vertical) pressure contour lines can be observed on the surface, suggesting that the flow is primarily two-dimensional. At $Re = 2.90 \times 10^5$, as shown in Fig. 4(b), these pressure contours no longer present two-dimensional flow. They demonstrate cell-like patterns near the regions close to midspan where rings are more densely arranged (hence there are more data points to plot the contours). These cell-like patterns were also observed in the surface pressure contours by Higuchi, *et al.* (1989) at a lower Reynolds number of 1.95×10^5 . In the current study, however, these cell-like structures were not observed until at a higher Reynolds number reaching 2.95×10^5 . The slanted patterns and cell-like constant pressure regions, which corresponds to three-dimensionality in the flow structure, are more evident at $Re = 3.33 \times 10^5$ (within the TrBL1 regime) as shown in Fig. 4(c). The increase of the Reynolds number to 3.80×10^5 , where the second separation bubble is formed, results in a narrower three-dimensional region as depicted in Fig. 4(d). Further increment in Reynolds number again serves to shift the observed constant pressure cells toward the ends and consequently narrow three-dimensional flow region as shown in Fig. 4(e). The same behavior in the surface pressure contours can be seen at the largest Reynolds number tested, 5.85×10^5 in Fig. 4(f).

3.2. Flow separation angle

3.2.1. Determination of separation angle

It is now quite well known that adverse pressure gradient is the main cause of separation of flow over a body. It induces an opposite force against the motion of fluid and thus decreases the skin friction. The point where the skin friction vanishes and beyond which flow reversal occurs in a steady flow is marked as the flow separation point. In unsteady and oscillatory flow conditions such as the current study, however, different criteria have been used for the determination of the separation point. Despard and Miller (1971) proposed an empirical definition for an unsteady oscillatory separation point as the farthest upstream point within the entire cycle of oscillation, at which the wall shear-stress is non-positive. Sears and Telionis (1975) noted the lack of evidences to detect the point where wall shear-stress vanishes in unsteady oscillatory flows. Based on the above mentioned studies, Higuchi, *et al.* (1989) indicated that both the instantaneous wall shear-stress and flow direction data are necessary for the determination of oscillatory separation points in the cases such as the flow past a circular cylinder.

The accurate definition of separation angle in unsteady flows is not the main focus of the present paper. Therefore, the instantaneous flow separation points in the current study are simply defined as the mathematical inflection point of the surface pressure curves, which are obtained by the application of curve fitting to the surface pressure data. This approach has been successfully



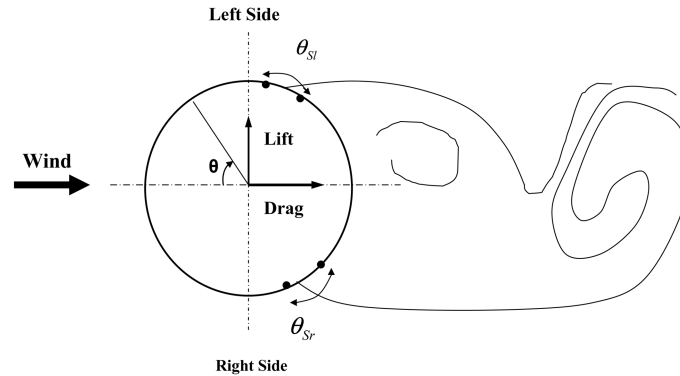


Fig. 5 Schematic and definition of left and right separation angles with respect to the on-coming wind direction

separation point from the fitted instantaneous surface pressure curves, the following criteria have been set: (a) The first derivative of the pressure curve with respect to θ at the corresponding point must be negative (i.e. it is located in the region of adverse pressure gradient); (b) The inflection point of the fitted curve, which represents the separation point, must be located within the expected region (i.e. $60^\circ \leq \theta \leq 150^\circ$ for the left separation angle, θ_{sl} , and $210^\circ \leq \theta \leq 300^\circ$ for the right separation angle, θ_{sr}); (c) The inflection point is located just after (or before in case of the right separation angle) the minimum pressure point, beyond which the adverse pressure gradient occurs. Following these criteria, the instantaneous separation angles are calculated and then time-averaged for further analyses.

3.2.2. Time-averaged separation angle

Fig. 6 shows the variation of time-averaged left separation angle, θ_{sl} , at each considered spanwise location versus Reynolds number. The figure also includes the results of Achenbach (1968) and Tani (1964). A general trend, at which θ_{sl} slightly increases with Re can be observed in all results within the sub-critical regime. While at higher Reynolds numbers ($Re > 3.5 \times 10^5$), when the separation bubbles form, Achenbach's (1968) results seem to overshoot and remain significantly higher than Tani's (1964) and the present results, while the latter two sets manifest better agreements.

Time-averaged separation angle calculated based on Ring 1 ($z/D = -10.5$) measurement experienced somewhat smoother variation with Re, i.e., the increase in the θ_{sl} value is less than those at other spanwise locations. Since Ring 1 is the closest ring to the top end plate, with a distance of 1D, the end plate might have somewhat diminished the expected increase in θ_{sl} . Therefore, the data obtained at $z/D = -10.5$ (Ring 1 location) will not be considered for further analyses (conducted in Section 3.3 to 3.5). Results of other rings showed more or less the expected variation for transitions to TrBL1 and TrBL2 regimes.

It can be detected from Fig. 6, that laminar boundary-layer separates almost uniformly along the cylinder span at $\theta_{sl} \approx 78^\circ$ at $Re = 1.14 \times 10^5$ and may rise slightly to $\theta_{sl} \approx 82^\circ$ at $Re = 2.33 \times 10^5$. Spanwise non-uniformities tend to begin around the upper limit of the TrBL0 regime, at which the spanwise cell-like structures are also observed in Fig. 4(b), suggesting the three-dimensional nature of the surrounding flow. The transition into TrBL1 regime was first identified in Fig. 3(b) to occur at some spanwise locations when Re reached 3.04×10^5 . This transition can not be detected from Fig. 6 by a considerable jump in θ_{sl} values, because the asymmetric surface pressure distribution

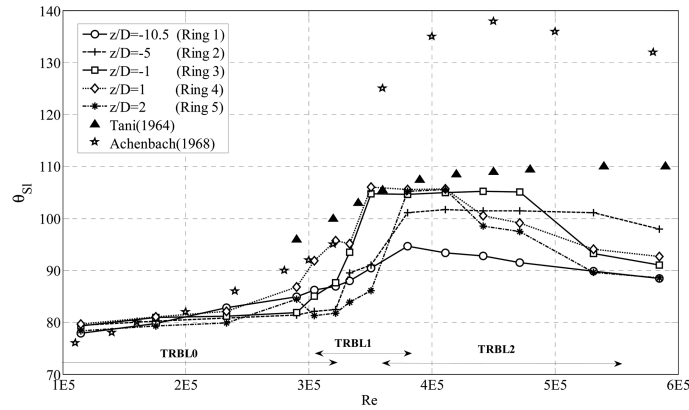


Fig. 6 Time-averaged separation angles on the left side of the cylinder; compared with Achenbach's (1968) and Tani's (1964) results

shown in Fig. 3(b) suggests that first separation bubble forms on the right side of the cylinder. The second transition, i.e., to the TrBL2 regime is detected first in Fig. 3(c) when $Re = 3.50 \times 10^5$ at $z/D = -1$ and 1 (Rings 3 and 4) and subsequently when $Re = 3.80 \times 10^5$ at $z/D = -5$ and 2 (Rings 2 and 5). This transition is accompanied by a jump of left separation angle to $100^\circ < \theta_{sl} < 105^\circ$ as seen in Fig. 6. Within TrBL2, the left separation angle gradually decreases to $89^\circ < \theta_{sl} < 97^\circ$ as the Reynolds number reaches 5.85×10^5 . This decrease seems to correspond to entrance into TrBL3 regime as the decrease of the minimum pressure coefficients in Fig. 3(d) appears to support this idea.

It thus appears that the observed jumps in the variation of separation angles occur at slightly different Reynolds numbers for different spanwise locations. In other words, the surface pressure distributions shown in Fig. 3, and the time-averaged separation angles, suggest that the respective overlaps of TrBL1 regime with TrBL0 and TrBL2 at its lower and upper limits exist, as illustrated in Fig. 6. This seems to verify Schewe's (1983) suggestion of which the flow could be divided along the span into different sub-systems, with each of them exhibiting slightly different characteristics corresponding to the co-existence of different flow sub-regimes. In the current study, TrBL1 regime is thus considered as the Reynolds number range within which any circumferential asymmetric pressure distribution exists along the cylinder span, i.e., $3.04 \times 10^5 < Re < 3.80 \times 10^5$ (also see Fig. 3).

Using flow visualization techniques, in addition to laminar separation angles, Tani (1964) also indicated the circumferential position where the transition into turbulence occurs within the critical range, i.e., $\theta \approx 90^\circ$ for TrBL0 regime and $\theta \approx 110^\circ$ for TrBL1 and TrBL2. The reattachment of boundary layer was also reported to occur at $\theta \approx 117^\circ$ within the TrBL1 regime. Achenbach (1968) used skin friction measurement which would give the final turbulent separation point around the circular cylinder. This could be the main reason for Achenbach's (1968) θ_s values to be larger than those of Tani's (1964) and the current study within the TrBL1 and TrBL2 regimes, as observed in Fig. 6. Despite the discrepancy with Achenbach's results (1968), the separation angles obtained in the current study exhibited all other expected features of transition into the TrBL1 and TrBL2 regimes. Therefore, they were used in the further analyses to study the three-dimensional flow structure around the circular cylinder. Comparing the current results with those of Achenbach's (1968) and Tani's (1964), it may be concluded that the proposed criteria for the detection of separation angles (i.e. curve fitting to the surface pressure data and locating inflection point of

curves) have led to the determination of the laminar separation point within the TrBL1 and TrBL2 regimes.

3.2.3. Power spectra of separation angle

Power spectral analysis is conducted for the time-histories of left and right separation angles, and the resulting power spectra are presented in Figs. 7 to 10, where the frequency domain f is normalized by V/D (free stream velocity divided by cylinder diameter). Normalized frequency of vortex shedding, the dominant frequency in the power spectra where the energy is concentrated, yields the Strouhal number, $St = f_s D/V$, where f_s is the Kármán vortex shedding frequency. Also, the third axis in Fig. 7 and Fig. 9 represents the spanwise distance from each ring to the cylinder mid-span. The power spectra density (PSD), as shown in Fig. 7 and Fig. 9, is obtained from the low sampling frequency data at Reynolds numbers of 1.75×10^5 to 3.33×10^5 at $z/D = -5, -1, 1, 2$ (Rings 2-5). High sampling frequency data set is used at higher Reynolds numbers of 3.50×10^5 to 5.85×10^5 at $z/D = -5, 1$ (Rings 2 and 4) to obtain power spectra in Fig. 8 and Fig. 10. The entire separation angle time-history was divided into equal segments, with Fast Fourier Transform (FFT) applied to

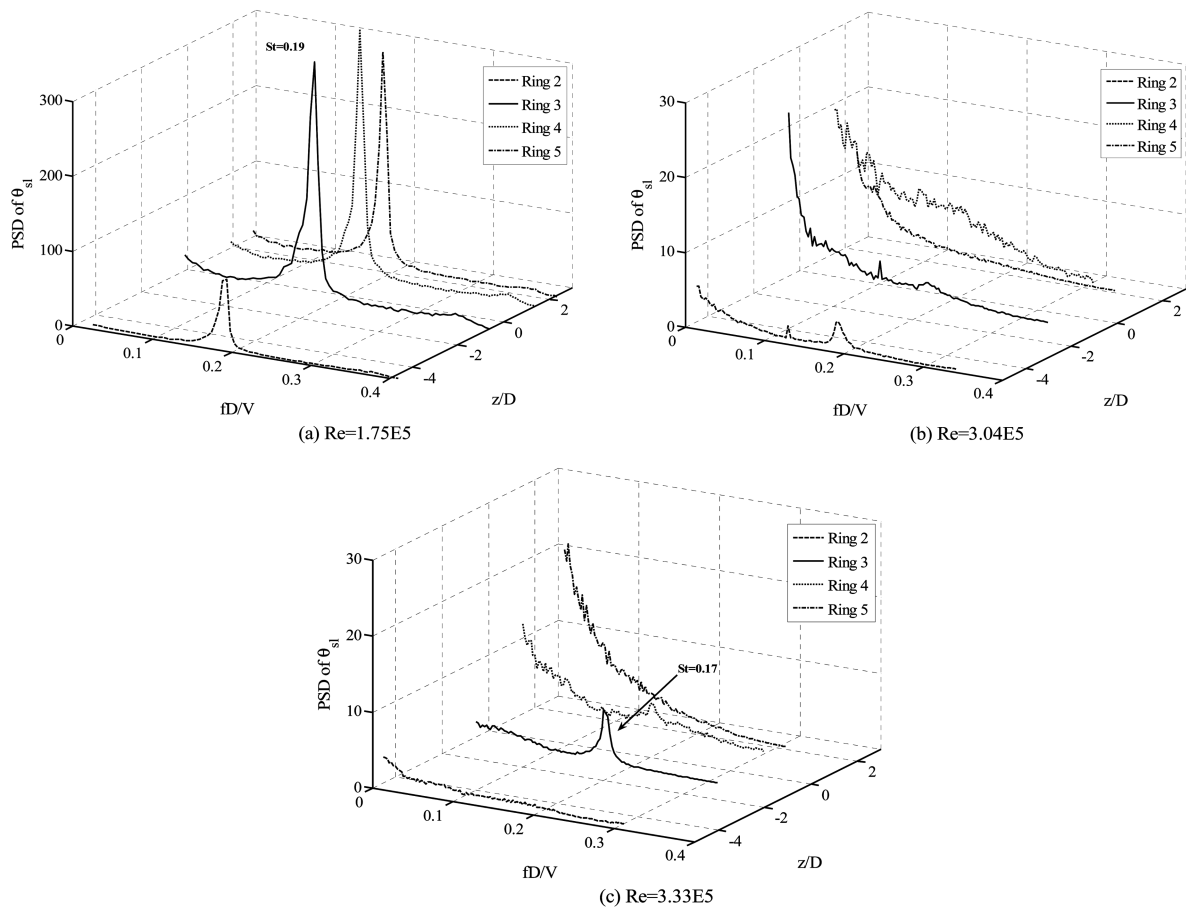


Fig. 7 Power spectra density of left separation angle on the cylinder at (a) $Re = 1.75E5$, (b) $Re = 3.04E5$, (c) $Re = 3.33E5$ at Rings 2-5, using low sampling frequency data

each of them. The obtained power spectra were then averaged to represent the energy distribution at different frequencies for the flow separation angle. It was found that 64 segments worked the best, i.e., resulted in smooth variation of PSD with distinct frequency peaks.

As shown in Fig. 7(a) and Fig. 9(a), left and right separation angles oscillate with very well-defined periodicity in the sub-critical regime, the dominant peaks suggest Strouhal number of 0.19 at all four spanwise locations. Another minor peak may also be detected at $2St$. The presented results are fairly consistent with other Strouhal number measurements in the sub-critical regime, such as Nishimura and Taniike (2001), who reported $St = 0.202$ at $Re = 6.1 \times 10^4$, and Bearman (1969), who reported $St = 0.18\text{--}0.20$ (using hot-wire signals) within this range. Strongly uniform distribution of separation angle PSD along the span of the cylinder highlights the two-dimensional and organized flow patterns within the sub-critical range.

Entrance to TrBL1 regime is denoted by lower energy level and broader energy distribution in the power spectra (say an order of magnitude lower than that of the sub-critical regime) and lack of spanwise uniformity comparing to the sub-critical regime, as shown in Fig. 7(b) and Fig. 9(b). Within the TrBL1 regime, energy is more concentrated in lower frequencies, however, minor peaks at $z/D = -5$ (Ring 2) can be detected at $St = 0.19$ both in Fig. 7(b) and Fig. 9(b). As conceived earlier from Fig. 3(b), at $Re = 3.04 \times 10^5$, jump in the surface pressure coefficient values at $z/D = -10.5, 1, 2$ (Rings 1, 4 and 5) occurs first on the right side of the cylinder. Compared to Fig. 9(b), relatively higher energy level shown in Fig. 7(b) at $z/D = 1$ and 2 (Rings 4 and 5) indicates that the formation of a single separation bubble on the cylinder surface would decrease the amount of separation angle fluctuation energy on the corresponding side more than the opposite side. In Fig. 7(c) and Fig. 9(c), at $Re = 3.33 \times 10^5$, detectable peaks at slightly lower Strouhal number of 0.17 can be observed in the PSD of the left and right separation angles at $z/D = -1$ (Ring 3). At this Reynolds number, energy distribution in the PSD of the right separation angles show lower levels than those of the left separation angles, except at $z/D = -1$ (Ring 3), where a considerably higher energy level corresponding to the peak of the right separation angle PSD is observed, as can be clearly seen in Fig. 9(c).

At higher Reynolds numbers, power spectra analysis of separation angle are conducted based on the high sampling frequency data set at $z/D = -5, 1$ (Rings 2 and 4) and presented in Fig. 8 and Fig.

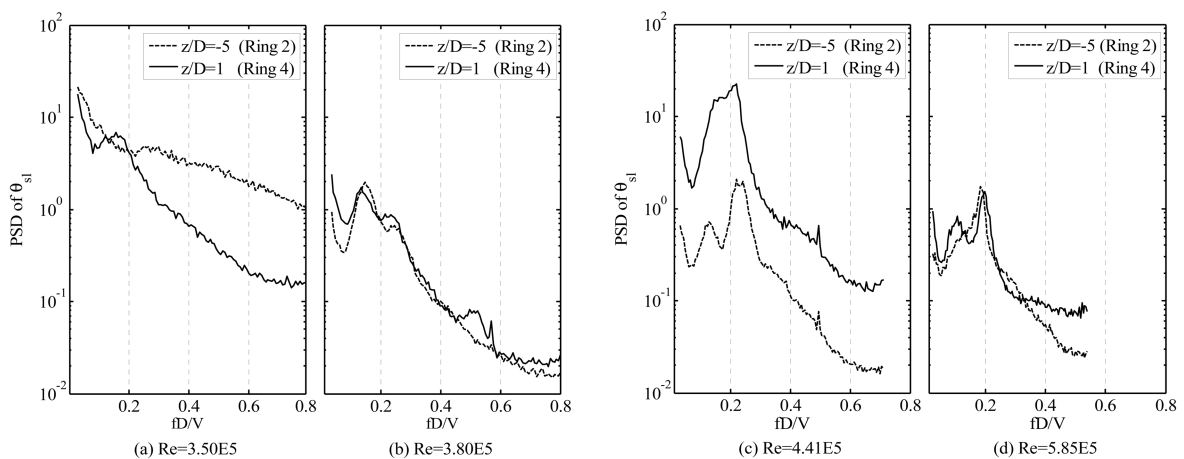


Fig. 8 Power spectra density of left separation angle on the cylinder at (a) $Re = 3.50E5$, (b) $Re = 3.80E5$, (c) $Re = 4.41E5$, (d) $Re = 5.85E5$ at Rings 2&4, using high sampling frequency data

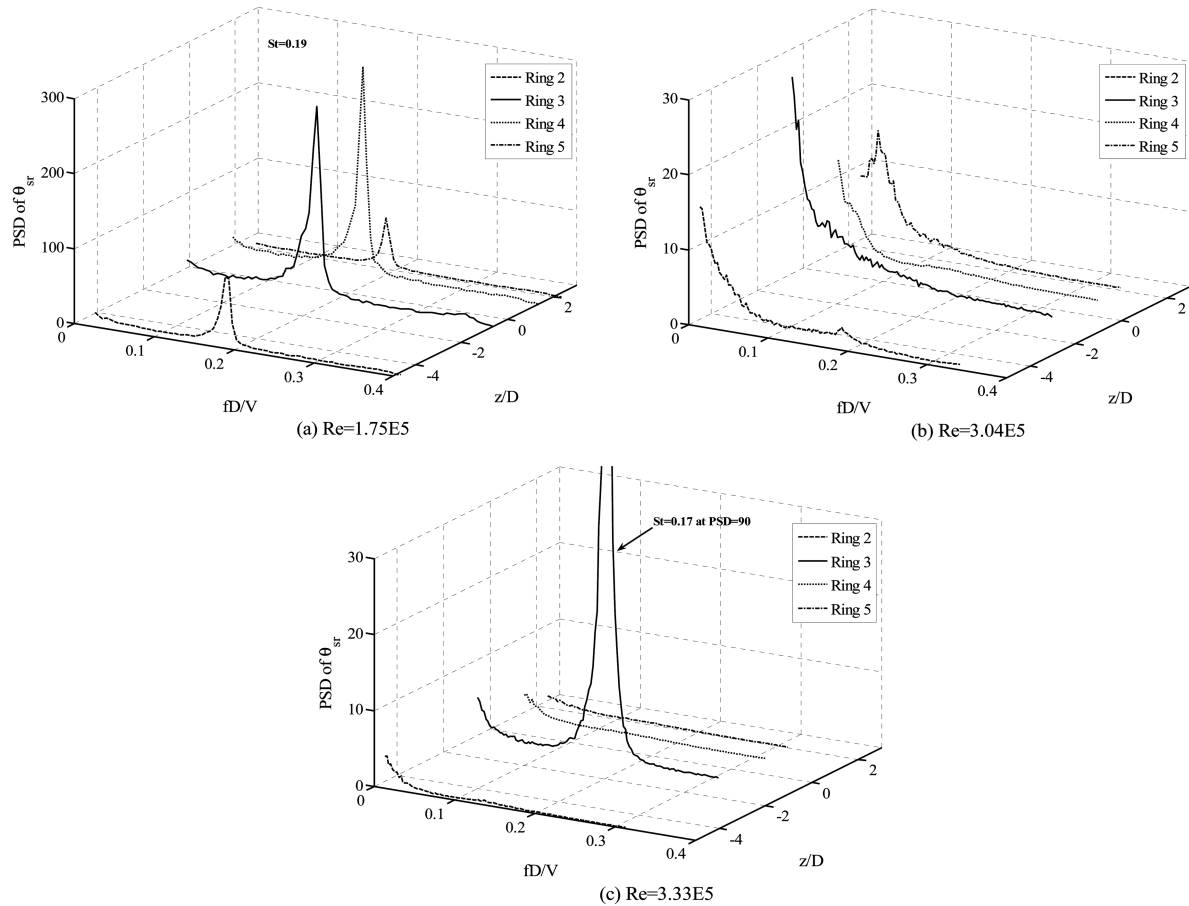


Fig. 9 Power spectra density of right separation angle on the cylinder at (a) $Re = 1.75E5$, (b) $Re = 3.04E5$, (c) $Re = 3.33E5$ at Rings 2-5, using low sampling frequency data

10. Entrance into the TrBL2 regime at all four spanwise locations occur when Re reaches 3.80×10^5 , as noted earlier. It can be observed in Fig. 8(b) and Fig. 10(b) that this transition results in another decrease in the energy level. Within the TrBL2 regime, qualitative trends in PSD of θ_{sl} and θ_{sr} are somewhat similar, suggesting the return of circumferential symmetry, though a lack of precisely quantitative agreement between the right and left separation angle power spectra can be seen in Fig. 8 and Fig. 10.

At $Re = 5.85 \times 10^5$, as depicted in Fig. 8(d) and Fig. 10(d), the PSD curves exhibit peaks at $St = 0.19$ at both spanwise locations. At this Reynolds number, however, relatively better spanwise agreement could be seen in terms of power spectra energy levels and energy distribution in the frequency domain in Figs. 8(d) and 10(d). It should be noted that there is still a lack of spanwise uniformity, suggesting the three-dimensionalities in the surrounding flow structure.

3.3. Fluctuating flow characteristics

Standard deviation of the fluctuation of the left and right separation angles at $z/D = -5, -1, 1, 2$

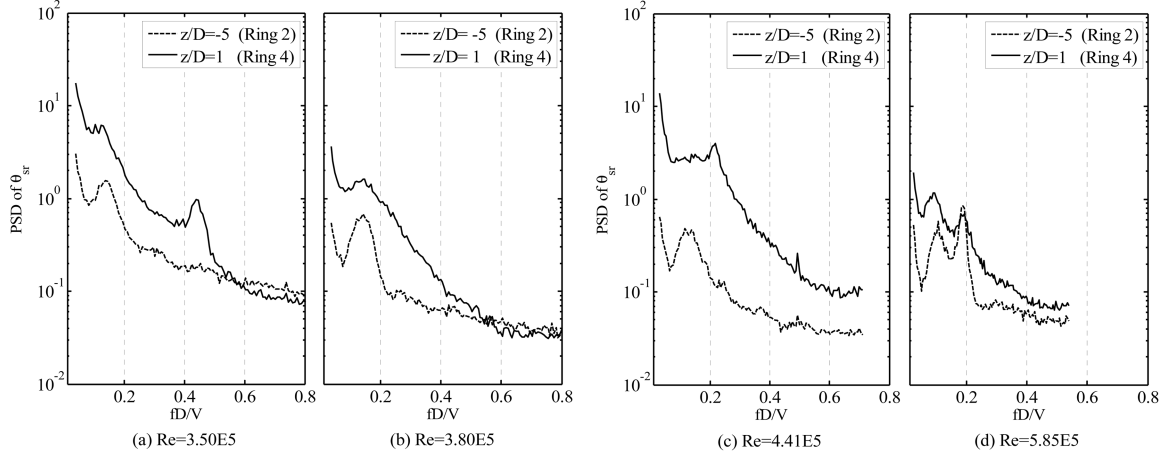


Fig. 10 Power spectra density of right separation angle on the cylinder at (a) $Re = 3.50E5$, (b) $Re = 3.80E5$, (c) $Re = 4.41E5$, (d) $Re = 5.85E5$ at Rings 2&4, using high sampling frequency data

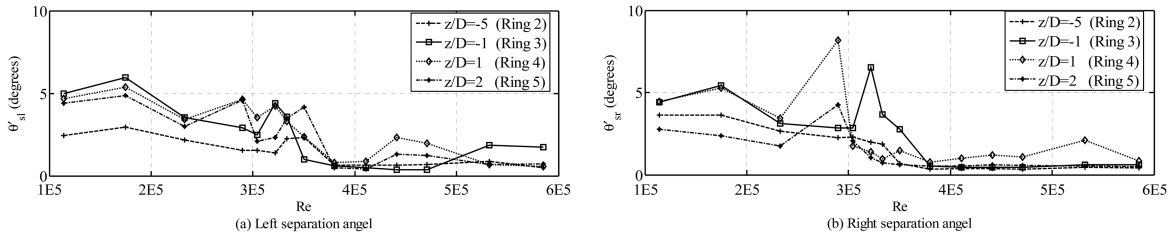


Fig. 11 Standard deviations of fluctuations of (a) left separation angle, (b) right separation angle for the studied Reynolds number range

(Rings 2-5) versus Reynolds number are presented in Fig. 11. A general trend, of which the fluctuation amplitude of the separation angles (θ_{sl} and θ_{sr}) decreases by increasing Reynolds number from the TrBL0 regime up to TrBL2 regime, can be seen in Fig. 11. The transition from TrBL0 into TrBL1 regime is accompanied by a decrease in the amplitude of fluctuations of the right separation angle at $z/D = -1, 1, 2$ (Rings 3-5), shown in Fig. 11(b), at the corresponding transition Reynolds number within the overlap range of TrBL1 (i.e. 3.04×10^5 Re 3.33×10^5). The same phenomenon, however at a lower degree, can be observed in Fig. 11(a) before the transition into TrBL2 regime. Based on the presented results, it might be concluded that the fluctuation amplitude of separation angles increases just before each transition into both TrBL1 and TrBL2 regimes and suddenly drops afterwards (i.e. θ_{sr} in case of transition into TrBL1 regime and θ_{sl} when transition from TrBL1 into TrBL2). At higher Reynolds number within the TrBL2 regime, the results show much smaller fluctuation amplitude of separation angles on both sides of the cylinder. This is probably related to the intermittent low amplitude movements of separation-reattachment bubble as indicated by Higuchi, *et al.* (1989).

Standard deviations of surface pressure at four circumferential locations ($\theta = 60^\circ, 90^\circ, 110^\circ, 150^\circ$) are normalized by their mean values (P' / P_{mean}) and plotted against Reynolds number, as illustrated in Fig. 12. At $\theta = 60^\circ$, as portrayed in Fig. 12(a), where the boundary layer is expected to be attached and laminar, strong spanwise agreement can be seen among the results at all spanwise locations except within the Re range of 3.04×10^5 to 3.80×10^5 , which was previously considered to be TrBL1 regime. This indicates that transition into TrBL1 regime could be detected from the

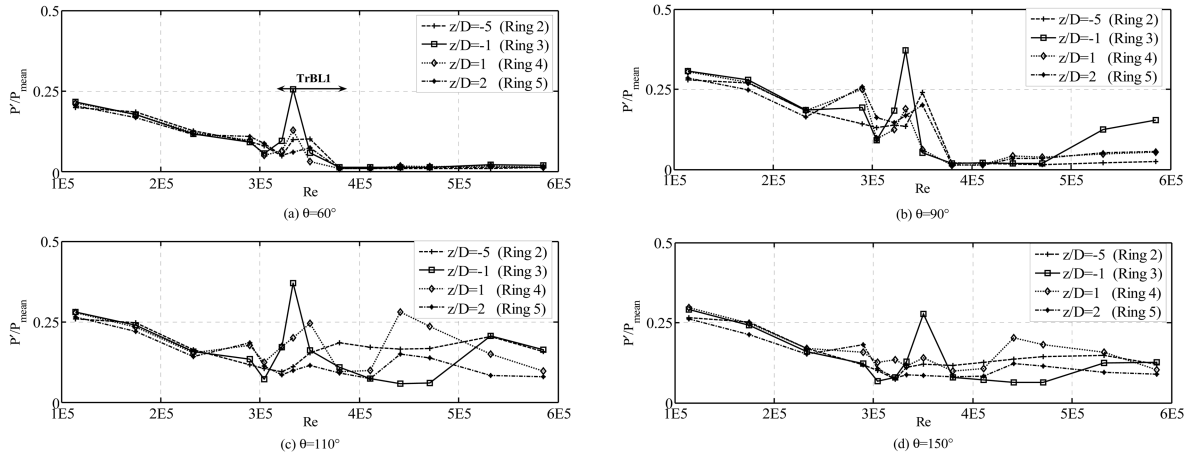


Fig. 12 Standard deviations of fluctuations of surface pressures at four angular locations, (a) $\theta = 60^\circ$, (b) $\theta = 90^\circ$, (c) $\theta = 110^\circ$, (d) $\theta = 150^\circ$; normalized with their mean values for the studied Reynolds number range

upstream of separation region in terms of disruption of spanwise uniformity of the flow. Fluctuating surface pressures at $\theta = 90^\circ$ are presented in Fig. 12(b), where the same behavior as that at $\theta = 60^\circ$ can be seen, except with higher amplitude and slightly more spanwise non-uniformity.

In Fig. 12(c), at $\theta = 110^\circ$, where the flow state is expected to be turbulent in the sub-critical range, there is still fairly good agreement among the results of all four spanwise locations for Re up to 2.33×10^5 . The largest discrepancy among the results of four rings can be seen at Reynolds numbers corresponding to the TrBL1 and TrBL2 regimes. Considering the time-averaged separation angle results from Fig. 6, this circumferential position ($\theta = 110^\circ$) is most likely located in the separation bubble and highly three-dimensional flow structure could be detected around its neighborhood. Fluctuation amplitude of surface pressure at $\theta = 150^\circ$ is presented in Fig. 12(d). Since it is located at the leeward side of the cylinder where the wake is present, the state of flow is expected to be turbulent over the entire tested Reynolds number range. Compared to Fig. 12(c), spanwise uniformity appears to be increased. Transitions to the TrBL1 and TrBL2 regimes, however, are not clearly distinguishable in Fig. 12(c) and 12(d) in terms of increase or decrease in the fluctuation amplitude like in Figs. 12(a)-12(b), except for those at $z/D = -1$ (Ring 3).

3.4. Spanwise correlations

Correlation coefficients of fluctuating separation angles, lift and drag forces, and surface pressures, are calculated and shown in Figs. 13-15. The dimensionless distances between different pairs of rings used in the correlation analysis are listed in Table 2. Fig. 13 shows the correlation coefficients of the separation angles at nine different Reynolds numbers within the tested range. The correlation coefficients decrease with the increase of spanwise distance at $Re = 1.75 \times 10^5$ within the TrBL0 regime. The same pattern can be observed in Fig. 14 and Fig. 15 at $Re = 1.75 \times 10^5$, for the variation of correlation coefficient of lift and drag, and surface pressure at $\theta = 110^\circ$ and $\theta = 150^\circ$.

Negative correlation coefficients is first identified at $Re = 2.90 \times 10^5$. It is then followed by very low correlation coefficients at $Re = 3.04 \times 10^5$ and $Re = 3.22 \times 10^5$ after the transition into TrBL1 regime, as can be observed in Figs. 13-15. Different patterns of correlation coefficient against spanwise

Table 2 Dimensionless distances between different pairs of rings

Pair of rings (<i>i, j</i>)	2,5	2,4	2,3	3,5	3,4	4,5
Dimensionless spanwise distance $z(i,j)/D$	7	6	4	3	2	1

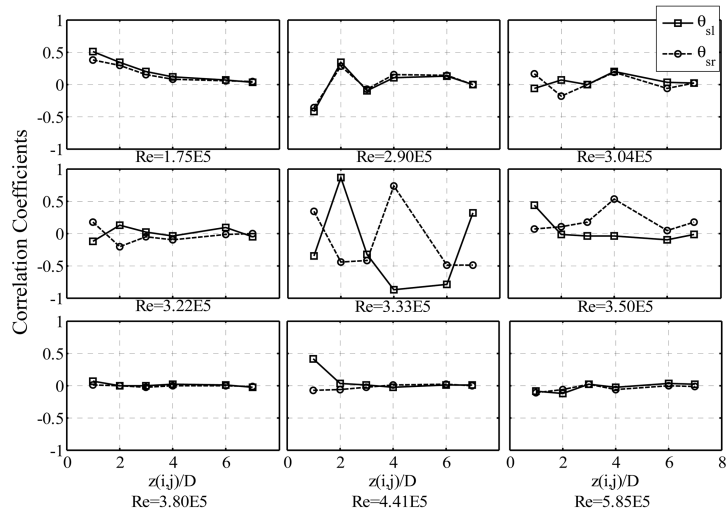


Fig. 13 Correlation coefficients of left and right separation angles

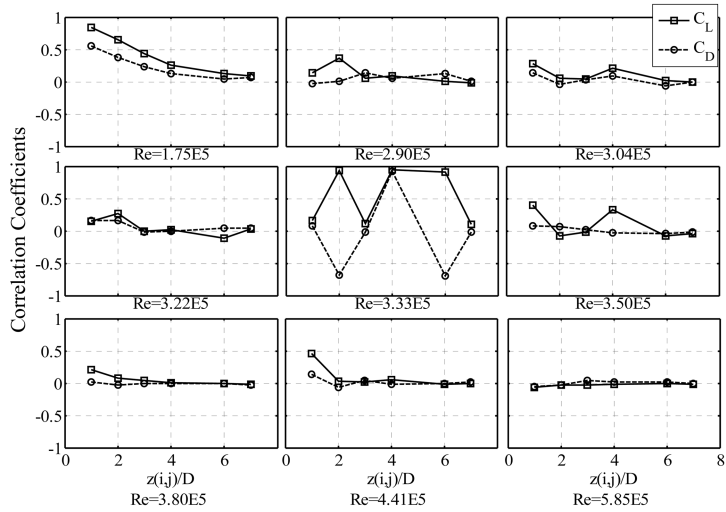


Fig. 14 Correlation coefficients of lift and drag coefficients

distance for $Re = 3.04 \sim 3.33 \times 10^5$, as illustrated in Fig. 13, indicates that within TrBL1 regime, spanwise distances of higher correlation coefficient tend to vary, which suggests that different flow structures exist along the cylinder span. Also, the in-phase and out-of-phase correlation coefficients of left and right separation angles between the same spanwise distances suggest that the separation lines on the left and right side of the cylinder surface have different patterns. This is particularly considerable at $Re = 3.33 \times 10^5$.

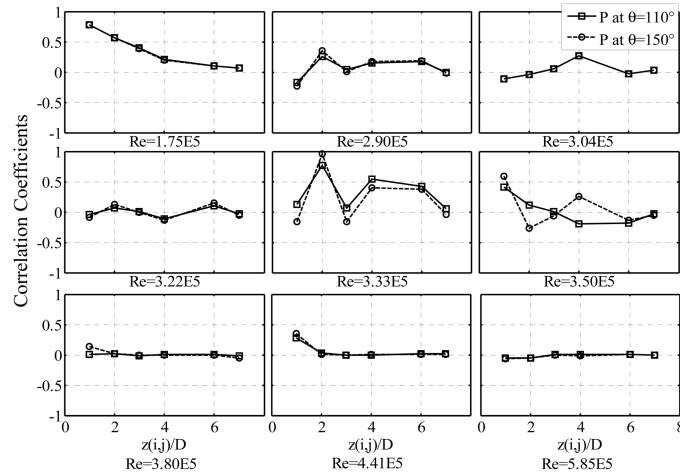


Fig. 15 Correlation coefficients of surface pressure at $\theta = 110^\circ$ and $\theta = 150^\circ$

Within TrBL1 regime, at $Re = 3.33 \times 10^5$, very large correlation coefficients, whether positive or negative, exist. This suggests very well-structured flow patterns around the cylinder at this Reynolds number. Very large in-phase correlation coefficients of the left separation angle, lift force, and surface pressures can be seen for spanwise distance of 2D, while right separation angle and drag force exhibit strong out-of-phase fluctuations for the same spanwise distance. It can also be seen in Figs. 14 and 15 that strong in-phase or out-of-phase correlation exists for spanwise distances of 2D, 4D and 6D; while for distances of 1D, 3D and 7D, almost zero correlation can be observed in the figures. It should be noted that there are no testing data available to conduct spatial correlation analysis for spanwise distance of 5D in the current study. The observed spanwise correlations suggest a size of the spanwise structures to be a multiple of two cylinder diameters at $Re = 3.33 \times 10^5$ within the TrBL1 regime. The spanwise regions of strong in-phase correlation have a size of 2D for lift force and 4D for drag force. At $Re = 3.33 \times 10^5$, the positive lift correlation coefficients suggests that there could be large overall instantaneous lift force acting on the cylinder, which is induced by the collaboration of the individual contributions from different spanwise structures. However, the summation of drag force correlation coefficients for different spanwise distances in Fig. 14 yields to almost zero, indicating that the overall drag force on the circular cylinder does not experience large instantaneous values, but rather relatively small fluctuation amplitudes.

The second transition occurs when reaching $Re = 3.80 \times 10^5$, which is the transition into TrBL2 regime marked by the formation of the second separation bubble. As observed from the third row of Figs. 13-15, the spanwise correlations of the fluctuating flow characteristics are almost lost, except for left separation angles, lift forces, and surface pressure at $Re = 4.41 \times 10^5$ when the two considered spanwise locations are separated only by one cylinder diameter. This is probably caused by the formation of the second separation bubble on the left side of the cylinder surface which leads to intermittent fluctuations in the flow characteristics and thus, very poor correlation strength.

3.5. Further discussion of spatial flow structure

It is now quite well-known that flow in the critical Reynolds number regime is extremely sensitive

to flow conditions and experiment setup (Bearman, 1969). Different sub-regimes may emerge or disappear at different Re values, due to variation in experimental details such as free stream turbulence and model surface roughness. It should also be noted that by monitoring different spanwise locations, the Reynolds number range of TrBL1 regime and the overlap ranges could vary. This somewhat explains the differences among the results of different researchers within the critical regime.

As discussed earlier (see Sections 3.2.3. and 3.3.), an increase-decrease manner in the fluctuating characteristics amplitudes (Figs. 11-12) and the energy levels in the power spectra of fluctuating separation angles (Figs. 7-10) is observed just before and after each transition to TrBL1 and TrBL2 regimes. It is proposed that within the TrBL1 regime, by increasing Reynolds number, the flow regains energy while the circumferential location at which transition of boundary-layer into turbulent state occurs, is kept more or less constant within the separation bubble (e.g. as suggested by Tani, 1964, to happen at $\theta = 110^\circ$). It leads to a better organized flow structure represented by relatively higher energy levels of PSD, fluctuation amplitudes and spanwise correlations (see Figs. 7, 9, 11-15).

In addition, stable spanwise structures have been reported in a few literatures. Humphreys (1960) identified it by using silk threads attached to the stagnation point at Reynolds numbers as low as 10^5 . At the supercritical regime, Korotkin (1976) found some spanwise non-uniformity just before and in the region of separation. Further experiments by Dallman and Schewe (1987) using oil-film flow visualization, pressure measurements by Higuchi, *et al.* (1989), and more recent work by Gölling (2004), showed cell-like patterns in flow structure with different cell sizes of 1.5 to 3.3 times of cylinder diameters in different studies. In the current study, the surface pressure contours presented in Fig. 4 show no more traces of the two-dimensional constant pressure patterns in the critical Reynolds number regime but rather, cell-like constant pressure regions surrounded by wave-shaped contours. These cell-like structures are observed to form mostly within the circumferential regions between $\theta = 60^\circ$ to $\theta = 100^\circ$ and have relatively lower pressure at the center of the cell. A very small region of favorable pressure gradient (as can be seen in Fig. 4) within these cell-like patterns decreases the opposite force against the boundary-layer motion and thus delays the flow separation. As can be seen in Figs. 4 and 6, at spanwise locations and Reynolds numbers which correspond to observed cell-like structures, flow separation is slightly delayed.

Within the sub-critical regime, the spanwise time-averaged separation angles (Fig. 6) and their amplitude of fluctuation (Figs. 11 and 12) are detected to be more or less constant. Considering the correlation coefficients in the sub-critical regime ($Re = 1.75 \times 10^5$ in Figs. 13-15), it implies that the separation lines along the cylinder span in the sub-critical regime are straight lines, or wave-shaped with very large wavelength, oscillating around their time-averaged values with almost the same amplitudes.

The observed three-dimensionalities in the flow within TrBL1 regime can also be discussed on the basis of the fluctuating component of surface pressures (Fig. 12). Transition into TrBL1 regime could be characterized at all angular positions considered ($\theta = 60^\circ, 90^\circ, 110^\circ$, and 150°) by the presence of spanwise non-uniformity in the fluctuating component of surface pressure. Even at the upstream region of $\theta = 60^\circ$, where the boundary layer is expected to be attached and laminar, the spanwise non-uniformity can be observed within the TrBL1 regime. This implies that strong three-dimensional flow structure around the circular cylinder in this range is associated with different circumferentially symmetric or asymmetric flow structures along the span of circular cylinder. Consequently, it could be observed that a large circumferential area of the cylinder is affected in the TrBL1 regime in terms of disruption of spanwise uniformity, while in the TrBL2 regime, the lack of spanwise uniformity

could be seen in a narrower circumferential area. However, this effect only lasts to the upper limit of the TrBL1 regime. Another three-dimensionality in the flow structure can be detected from the surface pressure fluctuation amplitude at $\theta = 110^\circ$ and $\theta = 150^\circ$ within the TrBL1 and TrBL2 regimes (in Figs. 12(c) and 12(d)). Within this circumferential range, the largest spanwise non-uniformities are seen at $\theta = 110^\circ$, where it is expected to be located within the separation bubble. This effect which endures within the TrBL2 regime indicates a different type of three-dimensionalities. It was suggested by Higuchi, *et al.* (1989) that the interactions of the separation-reattachment bubble that involves intermittent movement of the separation angles, has a great three-dimensional effect along the cylinder span. This effect is detected throughout Figs. 7-10 and Figs. 11-12 as long as separation bubbles exist on the cylinder surface (i.e. within TrBL1 and TrBL2 regimes).

4. Conclusions

Spatial structure of flow past a circular cylinder placed normal to the on-coming flow in the critical Reynolds number regime is investigated based on a set of wind tunnel experimental data. Instantaneous surface pressures sampled at five different locations along the cylinder span reveal the existence of the spanwise three-dimensional flow patterns in terms of cell-like structures at Reynolds numbers larger than 2.90×10^5 . The following main findings were obtained:

1. Two regions of overlap were found at both upper and lower limits of TrBL1 regime where the characteristics of dual flow sub-regimes were observed along the span of circular cylinder.
2. The three-dimensional structure of flow within the TrBL1 regime is found to be associated with different circumferentially asymmetric flow patterns along the cylinder span, in addition to the effect of intermittent motions within the laminar separation bubble.
3. The relatively strong spanwise correlation and hence organized flow structure, is observed before the transitions into the TrBL1 and TrBL2 regimes. Both transitions are marked with disruption of these organized flow structures.
4. Large positive, spanwise lift correlation coefficients at $Re = 3.33 \times 10^5$ implies that greater overall instantaneous lift force could be induced on the cylinder because of the collaboration of different spanwise sub-systems, which might potentially cause unstable flow-induced vibration.
5. Size of the spanwise sub-systems with in-phase fluctuations is found to be two cylinder diameters for lift force and four cylinder diameters for drag force.

Acknowledgement

This work is made possible by support of Natural Sciences and Engineering Research Council of Canada (NSERC). We are also grateful to National Research Council of Canada (NRCC).

References

- Achenbach, E. (1968), "Distribution of local pressure and skin friction around a circular cylinder in cross-flow up to $Re = 5 \times 10^6$ ", *J. Fluid Mech.*, **34**(4), 625-639.
- Batham, J. P. (1972), "Pressure distribution on circular cylinders at critical Reynolds numbers", *J. Fluid Mech.*, **57**, 209-228.
- Bearman, P. W. (1969), "On vortex shedding from a circular cylinder in the critical Reynolds number regime", *J. Fluid Mech.*, **37**, 577-585.
- Cheng, S. and Tanaka, H. (2005), "Correlation of aerodynamic forces on an inclined circular cylinder", *Wind*

- Struct., An Int. J.*, **8**(2), 135-146.
- Dallman, U. and Schewe, G. (1987). "On topological changes of separating flow structures of transition Reynolds numbers", *Proceedings of AIAA '19 Fluid Dynamics, Plasma Dynamics and Lasers Conference*, Honolulu, Hawaii, July.
- Despard, R. A. and Miller, J. A. (1971), "Separation in oscillating boundary layer flows", *J. Fluid Mech.*, **47**, 21-31.
- Fage, A. (1928). "The air flow around circular cylinder in the region where boundary layer separates from the surface", (*British Aero. Res. Coun., Rep. & Memo.*, **1179**).
- Farell, C. and Blessman, J. (1983), "On critical flow around smooth circular cylinders", *J. Fluid Mech.*, **136**, 375-401.
- Gölling, B. (2004), "Three-dimensional vortex flow of a circular cylinder", *Proceedings of the IUTAM Symposium on One Hundred Years of Boundary Layer Research*, DLR-Göttingen, Germany, August.
- Higuchi, H. Kim, H. J. and Farell, C. (1989), "On flow separation and reattachment around a circular cylinder at critical Reynolds numbers", *J. Fluid Mech.*, **200**, 149-171.
- Humphreys, J. S. (1960), "On a circular cylinder in a steady wind at transition Reynolds numbers", *J. Fluid Mech.*, **9**, 603-612.
- Korotkin, A. I. (1976), "The three dimensionality of the flow transverse to a circular cylinder", *Fluid Mechanics-Soviet Research*, **5**(2), 96-103.
- Nishimura, H. and Taniike, Y. (2001), "Aerodynamic characteristics of fluctuating forces on a circular cylinder", *J. Wind Eng. Ind. Aerodyn.*, **89**, 713-723.
- Norberg, C. (2001), "Flow around a circular cylinder: Aspects of fluctuating lift", *J. Fluid Struct.*, **15**, 459-469.
- Norberg, C. (2003), "Fluctuating lift on a circular cylinder: Review and new measurements", *J. Fluid Struct.*, **17**, 57-96.
- Roshko, A. (1954), "On the development of turbulent wakes from vortex streets", *NACA Report No.*, **TR1191**.
- Roshko, A. (1961), "Experiments on the flow past a circular cylinder at very high Reynolds number", *J. Fluid Mech.*, **10**, 345-356.
- Roshko, A. (1993), "Perspectives of bluff body aerodynamics", *J. Wind Eng. and Ind. Aerodyn.*, **49**, 79-100.
- Schewe, G. (1983), "On the force fluctuations acting on a circular cylinder in cross-flow sub-critical up to transcritical Reynolds numbers", *J. Fluid Mech.*, **133**, 265-285.
- Sears, W. R. and Telionis, D. P. (1975), "Boundary layer separation in unsteady flow", *SIAM J. Appl. Maths.*, **28**, 215-235.
- Simiu, E. and Scanlan, R. H. (1996), *Wind Effects on Structures: An Introduction to Wind Engineering*, 3rd Ed. John Wiley & Sons.
- Slaouti, A. and Gerrard, J. H. (1980), "An experimental investigation of the end effects on the wake of a circular cylinder towed through water at low Reynolds number", *J. Fluid Mech.*, **112**, 297-314.
- Tani, I. (1964), "Low speed flows involving bubble separations", *Prog. Aeronautical Science*, **5**, 70-90.
- Williamson, C. H. K. (1997), "Advances in our understanding of vortex dynamics in bluff body wakes", *J. Wind Eng. Ind. Aerodyn.*, **69-71**, 3-32.
- Zdravkovich, M. M. (1997), *Flow around Circular Cylinders, Fundamentals*, Vol. 1, University Press, Oxford, England.